Cetylpyridinium Trichlorostannate: Synthesis, Antimicrobial Properties, and Controlled-Release Properties via Electrical Resistance Tomography

Baran Teoman, Zilma Pereira Muneeswaran, Gaurav Verma, Dailin Chen, Tatiana V. Brinzari, Allison Almeda-Ahmadi, Javiera Norambuena, Shaopeng Xu, Shengqian Ma, Jeffrey M. Boyd, Piero M. Armenante, Andrei Potanin, Long Pan, Tewodros Asefa,* and Viktor Dubovoy*

Read Online

ACCESS | Metrics & More | Article Recommendations | Supporting Information

ABSTRACT: Cetylpyridinium trichlorostannate (CPC-Sn), comprising cetylpyridinium chloride (CPC) and stannous chloride, was synthesized and characterized via single-crystal X-ray diffraction measurements indicating stoichiometry of $C_{21}H_{38}NSnCl_3$ where the molecules are arranged in a 1:1 ratio with a cetylpyridinium cation and a $[SnCl_3]^-$ anion. CPC-Sn has shown potential for application as a broad-spectrum antimicrobial agent, to reduce bacteria-generated volatile sulfur compounds and to produce advanced functional materials. In order to investigate its controlled-release properties, electrical resistance tomography was implemented. The results demonstrate that CPC-Sn exhibits extended-release properties in an aqueous environment as opposed to the CPC counterpart.
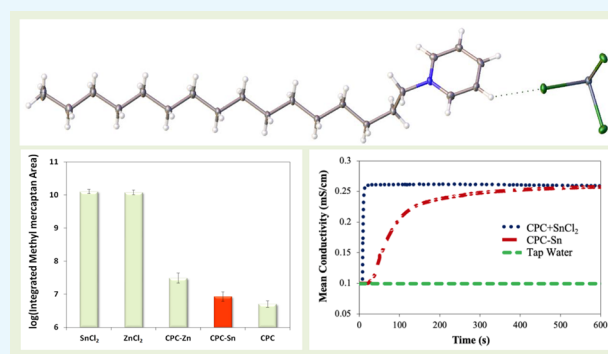
1. INTRODUCTION

Cetylpyridinium chloride (CPC) is a quaternary ammonium compound (QAC), with the stoichiometry $C_{21}H_{38}ClN$, which is widely used as an antibacterial cationic surfactant.[1] Its antimicrobial properties render it useful in a variety of applications including pharmaceuticals, water treatment, and some other industrial applications.[2−4] CPC is the active pharmaceutical ingredient (API) at 0.01−1% (w/w) of numerous healthcare products including oral rinses, dentifrices, throat and nasal sprays, dishwashing detergents, and lubricants.[1,5−7] It is recognized as a safe and effective active ingredient for dermal and oral applications by the Food and Drug Administration (FDA) in the United States, and it is commonly used in oral care products to prevent and treat dental plaque, gingivitis, halitosis, and calculus.[2,8−12]

The binding mechanism of CPC to the microbial cell membrane is composed of two simultaneously occurring steps: (1) the positively charged region of CPC binds directly to the polar negatively charged phosphate groups of phospholipids and (2) the nonpolar portion of CPC interacts with non-polar phospholipid tails. These steps result in permeability of the cell membrane, followed by membrane depolarization, leakage of intracellular components, and eventually the death of the microbial cell.[8,13] Thus, the interaction between a metal ion (e.g., Zn^{2+}) and CPC in a CPC−metal complex plays a crucial role in the antimicrobial efficacy of CPC.[14] Along with CPC, the metal ion should be readily bioavailable in order to quickly

and effectively bind to the microbial cell membrane, resulting in the high antimicrobial effect.

The antimicrobial effect of various metal ions (e.g., Cd^{2+}, Co^{2+}, Cu^{2+}, and Zn^{2+}) is thoroughly described elsewhere.[15−18] Moreover, the interaction between the metal ions and pyridine analogs has been specifically investigated by many researchers.[19−22] However, these studies were not successful in identifying and leveraging an antimicrobial technology that is viable, safe, and effective for widespread healthcare use. Recently, our group reported the synthesis and antimicrobial properties of cetylpyridinium tetrachlorozincate ($C_{42}H_{76}Cl_4N_2Zn$ = CPC-Zn) against various microbes (i.e., *Staphylococcus aureus*, *Streptococcus mutans*, and *Salmonella enterica*).[14] However, this study was limited to Zn that exhibits relatively weak bacteriostatic activity when compared to other divalent metal ions. It was postulated that the rational design of a CPC complex with a stronger bactericidal metal would improve the antimicrobial properties as compared to cetylpyridinium tetrachlorozincate. Thus, other metal ions could potentially be more efficient than Zn.
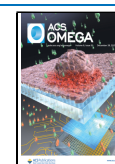
Among the potential metal ions that could substitute Zn, divalent tin [Sn(II)] is highly relevant, since it is known to exhibit low cytotoxicity and is frequently used in preservation, food packaging, electronics, and in the pharmaceutical industry (*e.g.*, SnF_2).[23,24] Several attempts have been made to investigate the antimicrobial properties of Sn(II) by dissolving its different forms (*i.e.*, SnF_2 and $SnCl_2$) or by forming thin films on the surface of glass that contains Sn(II) ions, all conforming that Sn(II) is a safe and effective antibacterial agent.[15,18,25,26]

Herein, we report the synthesis and characterization of cetylpyridinium trichlorostannate (CPC-Sn), which was found to have superior antimicrobial activity compared to CPC-Zn. Furthermore, previous work demonstrated that inorganic–organic hybrid advanced functional materials with controlled-release of QACs exhibit efficacious antimicrobial activity.[27] Controlled-release antimicrobial agents could be advantageously used in a variety of industrial and consumer product applications. Therefore, in this work, the controlled-release properties of CPC-Sn in an aqueous environment were investigated. To do so, a new methodology was developed based on a novel application of electrical resistance tomography (ERT).

ERT is a methodology that measures the electrical conductivity distribution within a specified region of a liquid by multiple electrode sensors that are directly immersed in the fluid. These electrodes inject electrical current into the liquid, one electrode pair at a time, measure the voltage resulting from the provided current, and construct a conductivity distribution map by deconvoluting the voltage signals.[28] Since the conductivity of liquid is directly correlated with the concentration of a polar solute, ERT can be used to quantify the distribution of those materials within the liquid. Due to its fast data acquisition characteristics, capability to conduct real-time process monitoring, and the advantage of providing local data at different locations of the bulk liquid, ERT has become a popular technique in the investigations of phase inversion,[29] precipitation,[30−32] flow distribution,[33,34] and mixing processes.[35−38] However, the use of ERT to study dissolution processes has been limited thus far. In fact, to the best of our knowledge, there have only been two reports of implementing ERT to investigate the dissolution process of salts.[39,40] In this report, ERT was used to monitor the dissolution of CPC, $SnCl_2$, and CPC-Sn in order to investigate the dissolution characteristics of these materials, as well as the controlled-release properties of CPC-Sn.

The current work reports the synthesis and characterization of cetylpyridinium trichlorostannate (referred to herein as CPC-Sn) that exhibits superior volatile sulfur compound (VSC) reduction properties as compared to CPC-Zn. Additionally, this study demonstrates that ERT is an efficient and reliable methodology to quantify the dissolution process of a wide variety of drug delivery systems (DDS), using CPC-Sn as a model. To the best of our knowledge, this is the first report in which ERT was used to characterize the dissolution of a bioactive compound.

2. MATERIALS AND METHODS

2.1. Synthesis of Cetylpyridinium Trichlorostannate (CPC-Sn).
Reagent grade $SnCl_2 \cdot 2H_2O$, cetylpyridinium chloride monohydrate, and absolute ethanol were supplied by Sigma-Aldrich (St. Louis, MO, USA) and used as supplied without further purification. Clear solutions of $SnCl_2 \cdot 2H_2O$ (10 wt %) and cetylpyridinium chloride monohydrate (25 wt %) were prepared in ethanol. Both samples were sonicated to ensure complete dissolution. It is noteworthy that the samples heated up quite a bit during the sonication (ca. 40−50 °C). A stannous chloride solution was added dropwise to the CPC solution. A crystalline "snowflake" material was formed after several minutes. This material was filtered, washed with copious amounts of water, and characterized via attenuated total reflectance-Fourier transform infrared spectroscopy (ATR-FTIR) and single-crystal X-ray diffraction (SC-XRD), as described below in detail.

2.2. Structural Characterization via ATR-FTIR.
The infrared spectra were collected using a Bruker Vertex 70 FTIR spectrometer (Bruker Optics, Billerica, MA) equipped with a GladiATR diamond ATR accessory (Pike technologies, Madison, WI). The spectral range was 80−4000 cm^{-1}, and a resolution of 4 cm^{-1} was used. All measurements were carried out at room temperature.

2.3. Structural Characterization via SC-XRD.
The X-ray diffraction data were collected at −173 °C using aBruker D8 Venture PHOTON 100 CPAD system equipped with a Cu Kα INCOATEC ImuS micro-focus source (λ = 1.54178 Å). Data integration and reduction were performed using SaintPlus 6.01.[41] Absorption correction was performed by a multi-scan method implemented in SADABS.[42] The space group was determined using XPREP implemented in APEX3.[43] The structure was solved using SHELXT (direct methods) and was refined using SHELXL-2019[44−46] (full-matrix least-squares on F2) through the OLEX2 interface program.[47] All non-hydrogen atoms were refined anisotropically. Hydrogen atoms were placed in geometrically calculated positions and were included in the refinement process using a riding model.

2.4. Volatile Sulfur Compound (VSC) Reduction.
Methyl mercaptan is a representative ingredient of volatile sulfur compounds (VSCs), which can be used as a marker for the quantitative measurement of mouth odor by gas chromatography-flame photometric detector technology. Sample preparation entailed dissolution of the $SnCl_2$, CPC, and CPC-Sn powders to a final concentration of 0.0075 wt %. Hydroxyapatite (HAP) disks were incubated with whole saliva to develop pellicles followed by the treatment of prepared solutions. After rinsing, the treated disks were transferred to headspace vials and incubated with VSC solution to mimic mouth odor VSC generation. The methyl mercaptan in the headspace was measured through gas chromatography, equipped with a flame photometric detector (GC-FPD). The results would enable the determination of the product's efficacy in mouth odor reduction.

2.5. Antimicrobial Assays.
The bacterial strains, growth conditions, and antimicrobial susceptibility assays were previously described elsewhere.[14]

2.6. Dissolution Characterization via Electrical Resistance Tomography (ERT).
An ITS P2+ ERT system (Industrial Tomography Systems PLC, Manchester, U.K.), comprising a linear rod probe with 16 electrodes connected to a data acquisition system (DAS) was used for tomographic conductivity measurements. The probe was fixed on the inner wall of a 600 mL beaker that was filled with tap water (40 °C). A magnetic stirrer rod was used to provide a continuous agitation of 600 rpm throughout all the experiments. In the DAS, 15 mA was set as the injection current, and the frequency of the current was 9600 Hz, similar to previous studies.[39,40,48] The ERT measurement speed was set to 2 frames/s, where one

frame included a matrix with a $10 \times 20 = 200$ local conductivity value across the ERT probe (*i.e.*, two-dimensional conductivity distribution). Since ERT is a technology that yields relative conductivity, an initial conductivity value of 0.1 mS/cm was set in the DAS for water, a reference frame was taken, and the measurements were started. Three experiments were conducted with 0.1 wt % NaCl solution to confirm the reproducibility.

The materials of interest, CPC + SnCl$_2$ (*i.e.*, physical mixture of CPC and SnCl$_2$·2H$_2$O powders) and CPC-Sn, each having a similar average particle size and a molar concentration of 0.00189 M, were added to the beaker containing water. However, CPC and SnCl$_2$ were pre-mixed in their powder form and then added at the same time to the beaker, whereas CPC-Sn was added by itself. Then, the mean conductivity data for the entire 2D plane were collected and plotted against time. By keeping all DAS settings constant and by following the same experimental procedure described above in all cases, several experiments were also conducted with different amount of CPC-Sn (0.05, 0.1, 0.15, and 0.2 wt %) in order to construct a calibration curve. A linear relationship between the mean conductivity and the concentration of dissolved species was separately obtained. During the actual dissolution experiments, the conductivity evolved over time from its base value to the same final value corresponding to the total dissolution of all species initially in the solids, irrespective of the dissolving species.[39]

The dissolution process was quantified by the analysis of the time trace of the normalized mean conductivity, χ, at each time t, calculated as

$$\chi(t) = \frac{\sigma(t) - \sigma_o}{\sigma(\infty) - \sigma_o} \qquad (1)$$

where $\sigma(t)$ is the instantaneous mean conductivity at any time t, σ_o is the reference mean conductivity, prior to the solute addition, and $\sigma(\infty)$ is the value of the conductivity at the end of the experiment when all particles were dissolved (*i.e.*, for $t \rightarrow \infty$). The normalized conductivity data were then analyzed using the diffusion-controlled dissolution model for spherical particles under "sink conditions" [referring to a dissolution process in which the solute concentration in the liquid bulk is much smaller than the saturated concentration, *i.e.*, the solubility value][49] suggested by Higuchi *et al.*[50] and represented by the following equation:

$$W_o^{2/3} - W(t)^{2/3} = k_{2/3} \cdot t \qquad (2)$$

In this equation, W_o is the initial particle mass, $W(t)$ is the mass of the undissolved particles at time t, and $k_{2/3}$ is the composite rate constant. This model has two-third dependency functionality on particle mass, and it has been used in previous studies.[51,52] To use this equation, we used the linear relationship between conductivity and solid concentration, representing a linear calibration curve described by

$$\frac{C(t) - C_o}{C_\infty - C_o} = \frac{\chi(t) - \chi_o}{\chi_\infty - \chi_o} \qquad (3)$$

where $C(t)$ is the molar solute concentration at a generic time t, C_o and C_∞ are, respectively, the initial and final molar concentrations, $\chi(t)$ is the mean conductivity at a generic time t, and χ_o and χ_∞ are the initial and final mean conductivity, respectively. Since the mass balance of the dissolving species

must be $W_o - W(t) = V \cdot C(t)$, where V is the volume of the media, eq 2 can be rewritten as

$$W_o^{2/3} - \left\{ W_o - V \left[C_o + \frac{\chi(t) - \chi_o}{\chi_\infty - \chi_o}(C_\infty - C_o) \right] \right\}^{2/3}$$
$$= k_{2/3} \cdot t \qquad (4)$$

Therefore, a plot of the left-hand side of the equation against time yields the value of the composite rate constant, $k_{2/3}$. Here, the initial and the final portions of the dissolution curves (indicating, respectively, that the dissolution has not fully started and that the sink condition assumption was no longer valid) were not considered in the analysis. Therefore, from a regression of the left-hand side of eq 4 vs time, using as input the experimental data, the value of the $k_{2/3}$ constant could be obtained as the slope. For both cases (dissolution of the CPC + SnCl$_2$ mixture and dissolution of CPC-Sn), $k_{2/3}$ was used to quantify the dissolution performances of the tested materials.

3. RESULTS AND DISCUSSION

3.1. Structural and Compositional Characterization.
The ATR-FTIR spectra of CPC·H$_2$O, SnCl$_2$·2H$_2$O, as-synthesized CPC-Sn, and previously synthesized cetylpyridinium tetrachlorozincate (CPC-Zn)[14] are shown in Figure 1.
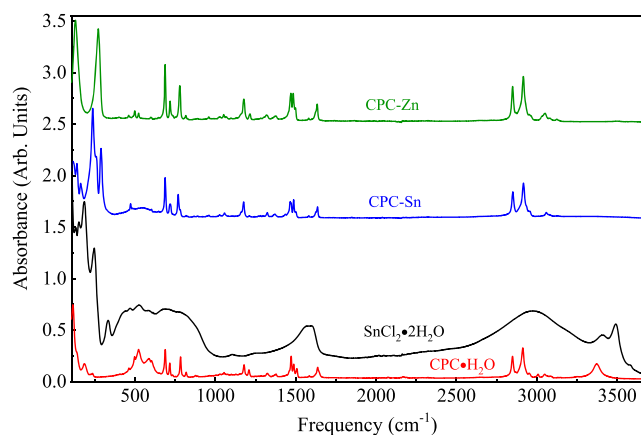

Figure 1. Comparison of the infrared absorption spectra for cetylpyridinium chloride monohydrate (CPC·H$_2$O), stannous chloride dihydrate (SnCl$_2$·2H$_2$O), CPC-Sn, and CPC-Zn.

The spectrum of the CPC-Sn sample clearly shows the fingerprint of the cetylpyridinium confirming its presence in the sample. A close inspection of the spectrum demonstrates that the bands of cetylpyridinium in CPC-Sn do not match those of the CPC·H$_2$O (*i.e.*, the precursor). The majority of the bands related to CH$_2$, C=C, C=N, and C−H stretching and cetylpyridinium bending vibrations display shifted peak positions compared to those of CPC·H$_2$O. The ν(OH) stretching band near 3370 cm^{-1} seen in the CPC·H$_2$O starting compound also disappears in the presence of Sn. Furthermore, a new cluster of bands below 340 cm^{-1} (*e.g.*, strong bands at 289, 260, and 237 cm^{-1}) is evident in the spectrum of the CPC-Sn sample, likely originating from the Sn-related vibrations. A comparison to the spectrum of SnCl$_2$·2H$_2$O does not reveal the presence of residual SnCl$_2$·2H$_2$O in the CPC-Sn sample. Finally, it is noteworthy that the spectra of CPC-Sn and CPC-Zn samples are overall similar in the behavior of the cetylpyridinium vibrational bands in the
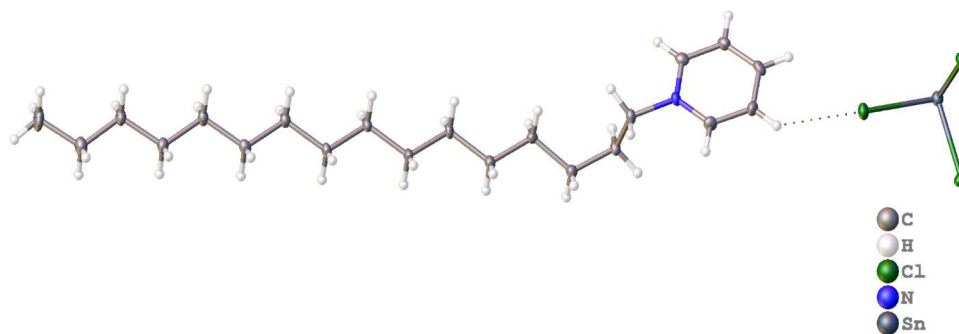
Figure 2. Asymmetric unit of CPC-Sn showing the CPC cation and the $SnCl_3^-$ anion.

(a)   **(b)**
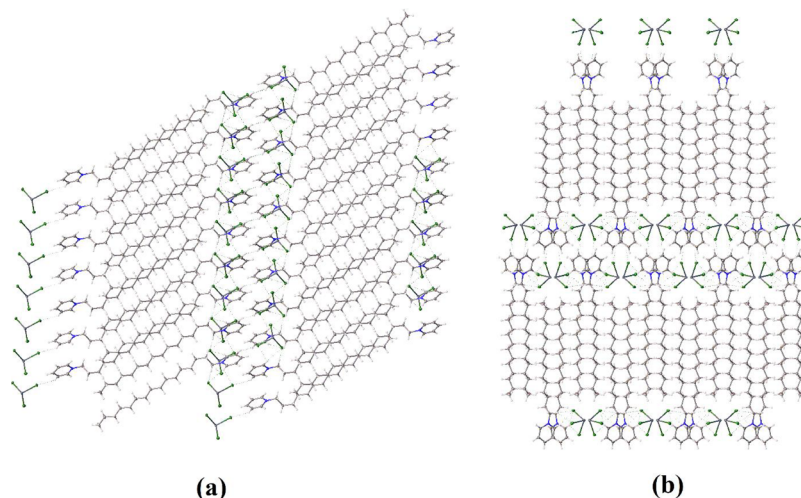
Figure 3. Packing along (a) the (010) plane and (b) the (001) plane of CPC-Sn.

presence of metal. Taken together, the FTIR data indicate the formation of a new compound occurred as a result of the reaction between CPC and $SnCl_2$.

After the initial discovery of the new compound formation from FTIR data, the sample was further analyzed by single-crystal X-ray diffraction. It is evident that the compounds are arranged in a 1:1 ratio with a cetylpyridinium cation and a $[SnCl_3]^-$ anion. The alkyl chains of CPC align with one another with the polar head groups facing in opposite directions for consecutive molecules. The pyridyl rings show a parallel stacking, and as a result of the packing arrangement, there is a non-polar region consisting of the stacked alkyl chains and a polar region consisting of the pyridinium rings and $SnCl_3^-$ anions.

The SC-XRD analysis reveals that the CPC-Sn crystallizes in the monoclinic $P21/c$ space group with the unit cell parameters a = 27.68(8) Å; b = 9.62(3) Å; c = 9.14(3) Å; and β = 92.95(10)°. The structural formula can be described as $[(C_{21}H_{38}N)][SnCl_3]$ or $(CP)SnCl_3$ with the asymmetric unit consisting of a cetylpyridinium cation and one $SnCl_3^-$ anion in distorted triangular pyramidal geometry (Figure 2). The positively charged pyridyl head is present in close contact with the negatively charged $SnCl_3^-$ unit via aromatic C—H———Cl hydrogen bonding interactions (d_{Cl--H} = 2.7 Å). The average Sn—Cl bond length is 2.48(7) Å, which is similar to other $SnCl_3^-$-based structures reported in the literature.[53,54] It is, however, worth noting that such kinds of hybrid organic–inorganic structures based on Sn(II) featuring independent $SnCl_3^-$ units are very rare in the literature.[55−58]

The packing of the compounds illustrated in Figure 3 shows stacked layers of interdigitated cetylpyridinium chains with the layers of $SnCl_3^-$ units present in between them. This gives rise to alternating cationic and anionic regions in the overall framework. This type of packing behavior is similar to other reported CPC structures,[59−64] albeit with a different packing arrangement.

The adjacent $SnCl_3^-$ units are aligned in opposite directions possibly due to repulsion between the Cl groups (Figure 4) with a Sn—Sn distance of 4.63 Å. The framework is stabilized by the hydrogen bonding interactions between the Cl from the anion and the aromatic as well as aliphatic C—H hydrogens on the CPC cation (−CH_2 attached to the pyridyl nitrogen, d = 2.77 Å). The $\pi-\pi$ interactions between the stacked phenyl rings are negligible as the distance between the centroids is greater than 4 Å. The selected bond lengths and angles for the structure are provided in the Supporting Information.

3.2. Volatile Sulfur Compound (VSC) Reduction. The effects of $ZnCl_2$, $SnCl_2$, CPC-Sn, CPC-Zn, and CPC on *in vitro* bacteria-generated volatile sulfur compounds (VSC), conducted by measuring the amount of methyl mercaptan in the headspace with gas chromatography (GC), are illustrated in Figure 5a. Statistical grouping, calculated using the Tukey method and a 95.0% confidence interval, indicates that CPC and CPC-Sn outperformed the other tested materials for malodor-causing VSCs with CPC and CPC-Sn exhibiting parity efficacy. Both CPC and CPC-Sn exhibited enhanced efficacy as compared to CPC-Zn. At the measured

(a)

(b)
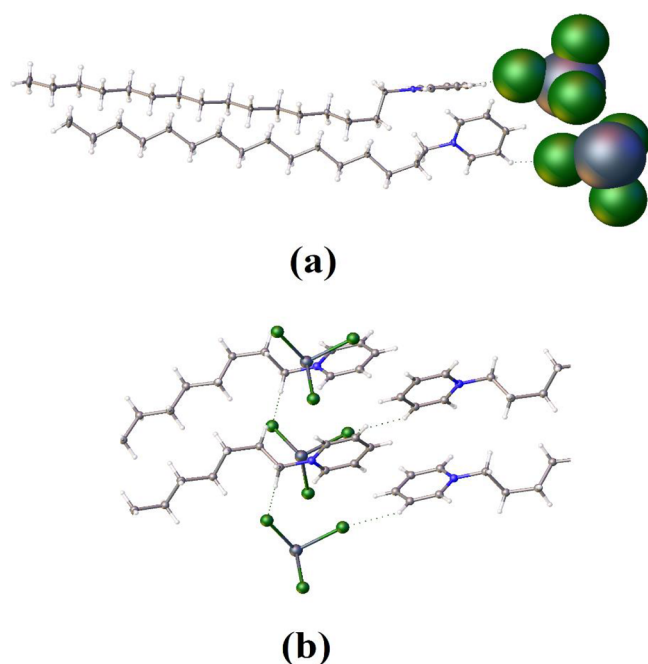
Figure 4. (a) Sphere packing diagram of the adjacent $SnCl_3^-$ units oriented in opposite directions and (b) hydrogen bonding interactions between the Cl from $SnCl_3$ and the aliphatic/aromatic C−H hydrogens.

concentrations, $ZnCl_2$ and $SnCl_2$ exhibit a weak VSC reduction effect as compared to CPC, CPC-Zn, and CPC-Sn.

3.3. Results of Antimicrobial Assays. The antimicrobial activities of CPC, CPC-Sn, and $SnCl_2$ were investigated against three human bacterial pathogens. A *Staphylococcus aureus* Los Angeles County clone (LAC) is a community-acquired methicillin-resistant *S. aureus* (MRSA) strain and a representative of the USA300 epidemic strain in the USA.[65] *Salmonella enterica* serovar Typhimurium is a leading cause of salmonellosis worldwide.[66] *Streptococcus mutans* is a leading cause of dental caries.[67] We individually cultured these bacterial strains with and without CPC, CPC-Sn, and $SnCl_2$ for 24 h and measured the cultures' optical densities. The amount of $SnCl_2$ required to inhibit growth with >100 μg mL^{-1} (data not shown) was above its solubility limit in water. It was difficult to determine an exact minimum inhibitory concentration (MIC) for $SnCl_2$ because of Sn(II) precipitation obfuscating the culture optical density readings. There was not a statistically significant difference in minimal inhibitory concentration (MIC) values between CPC-Sn and CPC in any of the three organisms examined (Figure 5b−d). The MIC values were approximately 13, 75, and 3 μg mL^{-1} for *S. aureus*, *S. enterica*, and *S. mutans*, respectively.

3.4. Results of Dissolution Experiments Using ERT. As previously mentioned, ERT was implemented to quantify the dissolution of the solute concentration as a function of time by measuring the corresponding normalized conductivity (eq 3). In all experiments, the initial conductivity of water was set to 0.1 mS/cm. Although stirring was incorporated, the con-
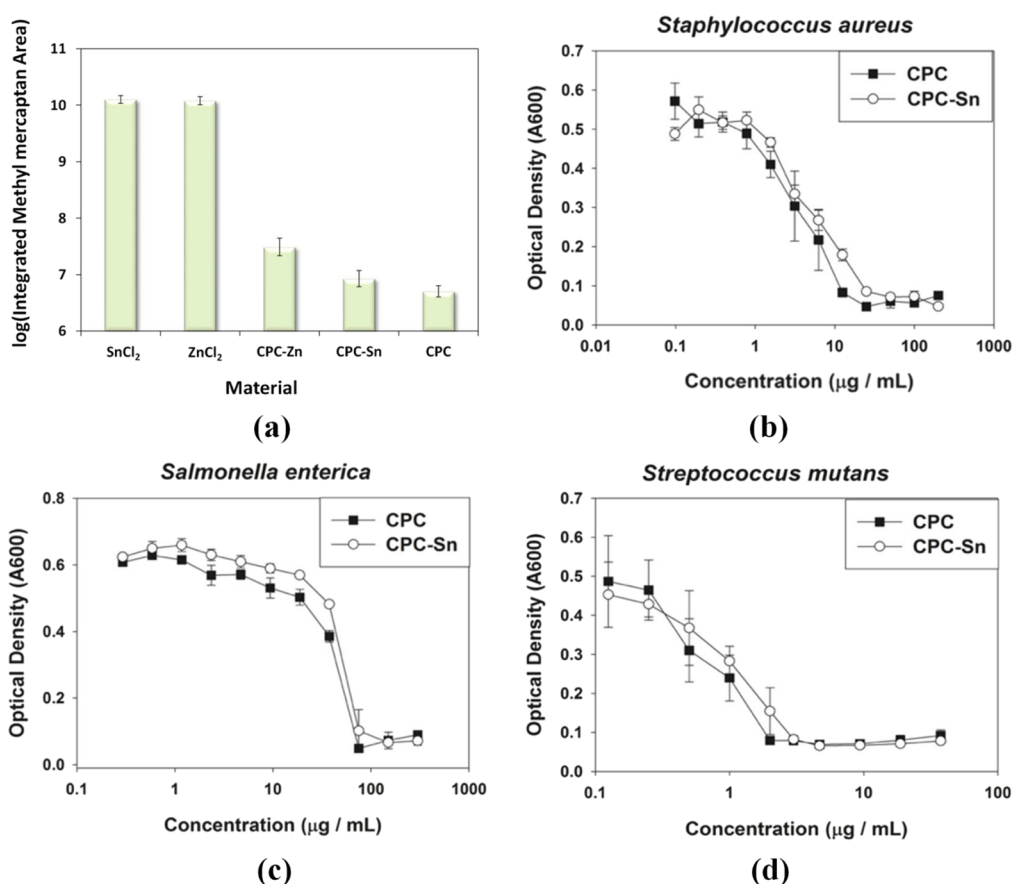
Figure 5. Inhibition of (a) methyl mercaptan by $SnCl_2$, $ZnCl_2$, CPC-Zn, CPC-Sn, and CPC and (b) *S. aureus*, (c) *S. enterica*, and (d) *S. mutans* with CPC and CPC-Sn.
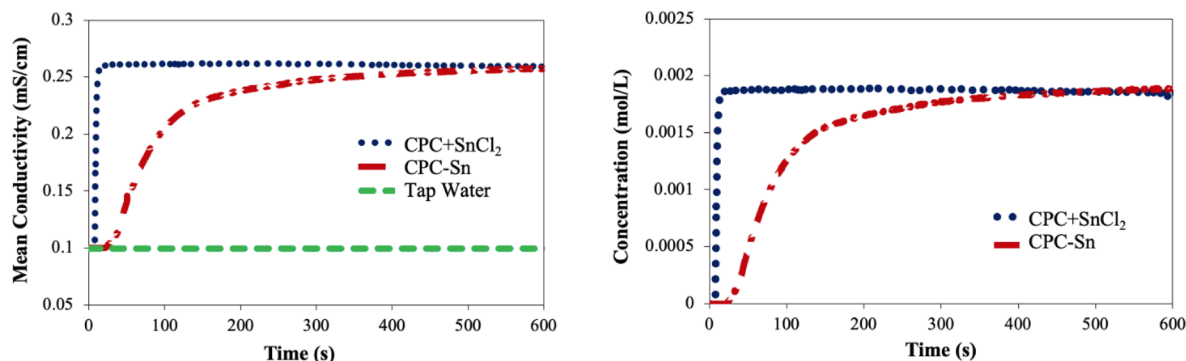
Figure 6. Dissolution curves obtained by ERT: (a) mean conductivity profiles for the CPC + SnCl$_2$ physical mixture, CPC-Sn, and tap water; and (b) concentration profiles for the CPC + SnCl$_2$ mixture and CPC-Sn.

ductivity remained constant over time (Figure 6a), indicating that the corresponding solute concentration in the solution was zero. In a typical experiment, the same amount (0.00113 mol) of either CPC + SnCl$_2$ powder mixture or CPC-Sn was added to the water while stirring. Upon complete dissolution of the solute, the final solute concentration was 0.00189 M in both cases since the ionic concentrations of the dissolved species were the same. Figure 6a shows the typical mean concentration profiles for both solutes. One can clearly see that the dissolution curves converged toward the same asymptotic value for $t \rightarrow \infty$ irrespective of the type of compound added initially.

Figure 6b shows the corresponding mean conductivity profiles for the CPC + SnCl$_2$ mixture and for CPC-Sn. Here, it is evident that the dissolution of the CPC + SnCl$_2$ mixture was essentially complete for $t \cong 20$ s, when the final concentration was reached (0.00189 M). However, the time for the complete dissolution of CPC-Sn was about 10 min.

While it is possible to visually distinguish between the dissolution rates of CPC-Sn and CPC + SnCl$_2$ by simple inspection of the dissolution curves, a more precise analysis can be conducted by quantifying the slope of the initial linearly increasing portions of the same curves. To do so, we applied the dissolution model of Higuchi and Hiestand (eq 2) to the dissolution profiles of the CPC + SnCl$_2$ mixture and CPC-Sn since this model accurately represents the dissolution profiles under sink conditions (Figure 7).[51,52] Here, the slopes of the linear portions of these curves yielded composite rate constants of $k_{2/3} = 0.0025$ mol$^{2/3}$/s and $k_{2/3} = 0.0001$ mol$^{2/3}$/s for the CPC + SnCl$_2$ mixture and CPC-Sn, respectively. These results clearly show that the initial dissolution rate of CPC-Sn was about 25 times less than that of the CPC + SnCl$_2$ mixture, although the final concentration of all dissolved species was the same in both cases, thus clearly showing the extended-release characteristics of CPC-Sn in an aqueous environment.

4. CONCLUSIONS

In this study, a novel CPC complex, cetylpyridinium trichlorostannate (CPC-Sn), was synthesized and unambiguously characterized via single-crystal X-ray diffraction indicating a stoichiometry of C$_{21}$H$_{38}$NSnCl$_3$ where the molecules are arranged in a 1:1 ratio with a cetylpyridinium cation and [SnCl$_3$]$^-$ anion. CPC-Sn exhibited superior antibacterial efficacy as compared to previously reported CPC analogs, especially evident in volatile sulfur compound (VSC) reduction experiments. Its dissolution characteristics, obtained from ERT, showed that CPC-Sn exhibits extended dissolution
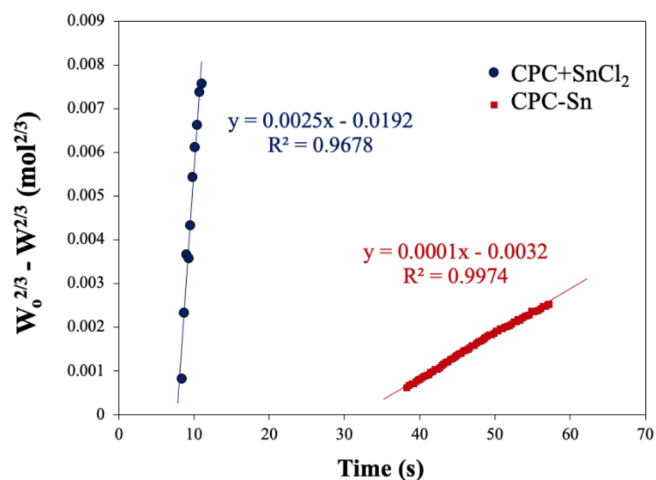
Figure 7. Application of the Higuchi and Hiestand (eq 2) dissolution model to the dissolution profiles of the CPC + SnCl$_2$ mixture and CPC-Sn under sink conditions, obtained from ERT.

as opposed to CPC in an aqueous environment. This work suggests that CPC-Sn is a viable and effective antimicrobial agent to combat the global healthcare issues associated with oral and dermal diseases, such as hospital infections, medical device biofilms, and antibiotic resistance. Furthermore, the novel application of ERT to investigate dissolution characteristics of bioactive molecules was demonstrated, which can be applied to a wide range of solutes.

■ ASSOCIATED CONTENT

ⓢ Supporting Information

The Supporting Information is available free of charge at https://pubs.acs.org/doi/10.1021/acsomega.1c04034.

> Crystallographic data of CPC-Sn (CIF)
> Experimental details and supporting results for the synthesis, structural characterization, and dissolution characteristics of CPC-Sn (PDF)

■ AUTHOR INFORMATION

Corresponding Authors

Tewodros Asefa − *Department of Chemistry and Chemical Biology, Rutgers, The State University of New Jersey, Piscataway, New Jersey 08854, United States; Department of Chemical and Biochemical Engineering, Rutgers, The State University of New Jersey, Piscataway, New Jersey 08854,*

United States; ● orcid.org/0000-0001-8634-5437;
Email: tasefa@chem.rutgers.edu

Viktor Dubovoy − Colgate-Palmolive Company, Piscataway,
New Jersey 08854, United States; ● orcid.org/0000-0001-
7661-0823; Email: vdubovoy@gmail.com

Authors

Baran Teoman − Colgate-Palmolive Company, Piscataway,
New Jersey 08854, United States; Otto H. York Department
of Chemical and Materials Engineering, New Jersey Institute
of Technology, Newark, New Jersey 07102, United States;
● orcid.org/0000-0001-5796-1054

Zilma Pereira Muneeswaran − Colgate-Palmolive Company,
Piscataway, New Jersey 08854, United States; Department of
Chemistry and Chemical Biology, Rutgers, The State
University of New Jersey, Piscataway, New Jersey 08854,
United States

Gaurav Verma − Department of Chemistry, University of
North Texas, Denton, Texas 76201, United States

Dailin Chen − Colgate-Palmolive Company, Guangzhou
510620, China

Tatiana V. Brinzari − Colgate-Palmolive Company,
Piscataway, New Jersey 08854, United States

Allison Almeda-Ahmadi − Department of Biochemistry and
Microbiology, Rutgers, The State University of New Jersey,
New Brunswick, New Jersey 08901, United States

Javiera Norambuena − Department of Biochemistry and
Microbiology, Rutgers, The State University of New Jersey,
New Brunswick, New Jersey 08901, United States

Shaopeng Xu − Colgate-Palmolive Company, Guangzhou
510620, China

Shengqian Ma − Department of Chemistry, University of
North Texas, Denton, Texas 76201, United States;
● orcid.org/0000-0002-1897-7069

Jeffrey M. Boyd − Department of Biochemistry and
Microbiology, Rutgers, The State University of New Jersey,
New Brunswick, New Jersey 08901, United States;
● orcid.org/0000-0001-7721-3926

Piero M. Armenante − Otto H. York Department of Chemical
and Materials Engineering, New Jersey Institute of
Technology, Newark, New Jersey 07102, United States;
● orcid.org/0000-0003-0753-1384

Andrei Potanin − Colgate-Palmolive Company, Piscataway,
New Jersey 08854, United States

Long Pan − Colgate-Palmolive Company, Piscataway, New
Jersey 08854, United States; ● orcid.org/0000-0003-0438-
4040

Complete contact information is available at:
https://pubs.acs.org/10.1021/acsomega.1c04034

Author Contributions

The manuscript was written through contributions of all
authors.

Notes

The authors declare no competing financial interest.

■ REFERENCES

(1) Nguyen, L. N.; Oh, S. Impacts of antiseptic cetylpyridinium
chloride on microbiome and its removal efficiency in aerobic activated
sludge. Int. Biodeterior. Biodegradation. 2019, 137, 23−29.

(2) Ash, M.; Ash, I. Handbook of Preservatives. Synapse Information
Resources: 2004.

(3) Imai, H.; Kita, F.; Ikesugi, S.; Abe, M.; Sogabe, S.; Nishimura-
Danjobara, Y.; Miura, H.; Oyama, Y. Cetylpyridinium chloride at
sublethal levels increases the susceptibility of rat thymic lymphocytes
to oxidative stress. Chemosphere 2017, 170, 118−123.

(4) Ko, C.; Huangb, C.; Hsieha, S.; Kuoc, P. Characterization of two
quaternary ammonium chloride-resistant bacteria isolated from
papermaking processing water and the biocidal effect on their biofilm
formation. Int. Biodeterior. Biodegradation. 2007, 60, 250−257.

(5) Costa, X.; Laguna, E.; Herrera, D.; Serrano, J.; Alonso, B.; Sanz,
M. Efficacy of a new mouth rinse formulation based on 0.07%
cetylpyridinium chloride in the control of plaque and gingivitis: a 6-
month randomized clinical trial. J. Clin. Periodontol. 2013, 40, 1007−
1015.

(6) Zhang, C.; Cui, F.; Zeng, G.; Jiang, M.; Yang, Z.; Yu, Z.; Zhu,
M.; Shen, L. Quaternary ammonium compounds (QACs): A review
on occurrence, fate and toxicity in the environment. Sci. Total Environ.
2015, 518-519, 352−362.

(7) Sundheim, G.; Langsrud, S.; Heir, E.; Holck, A. L. Bacterial
resistance to disinfectants containing quaternary ammonium com-
pounds. Int. Biodeterior. Biodegradation. 1998, 41, 235−239.

(8) Administration, U. F. A. D. Oral health care drug products for
over-the-counter human use; antigingivitis/antiplaque drug products;
establishment of a monograph; proposed rules. Federal Register. 2003,
68, 32247.

(9) Sreenivasan, P. K.; Haraszthy, V. I.; Zambon, J. J. Antimicrobial
efficacy of 0.05% cetylpyridinium chloride mouthrinses. Lett. Appl.
Microbiol. 2013, 56, 14−20.

(10) Liu, J.; Ling, J. Q.; Wu, C. D. Cetylpyridinium chloride
suppresses gene expression associated with halitosis. Arch. Oral Biol.
2013, 58, 1686−1691.

(11) Gibb, R.; Dunavent, J.; Flood, J.; Barnes, J.; Witt, J.; Ramji, N.
Antibacterial and antiplaque effects of a novel, alcohol-free oral rinse
with cetylpyridinium chloride. J. Contemp. Dent. Pract. 2005, 6, 001−
009.

(12) Rahardjo, A.; Ramadhani, A.; Adiatman, M.; Wimardhani, Y. S.;
Maharani, D. A. Efficacy of mouth rinse formulation based on cetyl
pyridinium chloride in the control of plaque as an early onset of
dental calculus built up. J. Int. Med. Res. 2016, 9, 184−188.

(13) Arrigler, V.; Kogej, K.; Majhenc, J.; Svetina, S. Interaction of
cetylpyridinium chloride with giant lipid vesicles. Langmuir 2005, 21,
7653−7661.

(14) Dubovoy, V.; Nawrocki, S.; Verma, G.; Wojtas, L.; Desai, P.;
Al-Tameemi, H.; Brinzari, T. V.; Stranick, M.; Chen, D.; Xu, S.; Ma,
S.; Boyd, J. M.; Asefa, T.; Pan, L. Synthesis, characterization, and
investigation of the antimicrobial activity of cetylpyridinium
tetrachlorozincate. ACS Omega 2020, 5, 10359−10365.

(15) Frei, A.; Zuegg, J.; Elliott, A. G.; Baker, M.; Braese, S.; Brown,
C.; Chen, F.; Dowson, C. G.; Dujardin, G.; Jung, N.; King, A. P.;
Mansour, A. M.; Massi, M.; Moat, J.; Mohamed, H. A.; Renfrew, A.
K.; Rutledge, P. J.; Sadler, P. J.; Todd, M. H.; Willans, C. E.; Wilson, J.
J.; Cooper, M. A.; Blaskovich, M. A. T. Metal complexes as a
promising source for new antibiotics. Chem. Eng. Sci. 2020, 11, 2627−
2639.

(16) Calomiris, J. J.; Armstrong, J. L.; Seidler, R. J. Association of
metal tolerance with multiple antibiotic resistance of bacteria isolated
from drinking water. Appl. Environ. Microbiol. 1984, 47, 1238−1242.

(17) Hobman, J. L.; Crossman, L. C. Bacterial antimicrobial metal
ion resistance. J. Med. Microbiol. 2014, 64, 471−497.

(18) Yasuyuki, M.; Kunihiro, K.; Kurissery, S.; Kanavillil, N.; Sato,
Y.; Kikuchi, Y. Antibacterial properties of nine pure metals: a
laboratory study using Staphylococcus aureus and Escherichia coli.
Biofouling 2010, 26, 851−858.

(19) Neve, F.; Francescangeli, O.; Crispini, A. Crystal architecture and mesophase structure of long-chain N-alkylpyridinium tetrachlorometallates. *Inorg. Chim. Acta* **2002**, *338*, 51−58.

(20) Hilp, M.; Zembatova, S. Cetylpyridinium tetrachlorozincate as standard for tenside titration. Analytical methods with 1,3-dibromo-5,5-dimethylhydantoin (DBH) in respect to environmental and economical concern, part 19. *Pharmazie* **2004**, *59*, 615−617.

(21) Hilp, M. Determination of anionactive tensides using cetylpyridinium tetrachlorozincate as titrant. Analytical methods in respect to environmental and economical concern, part 20. *Pharmazie* **2004**, *59*, 676−677.

(22) Kaur, G.; Kumar, S.; Dilbaghi, N.; Bhanjana, G.; Guru, S. K.; Bhushan, S.; Jaglan, S.; Hassan, P. A.; Aswal, V. K. Hybrid surfactants decorated with copper ions: aggregation behavior, antimicrobial activity and anti-proliferative effect. *Phys. Chem. Chem.* **2016**, *18*, 23961−23970.

(23) Buyukakinci, B. Y. Investigation of antibacterial activities of tin ions on wool fabric. *Ind. Textila* **2013**, *5*, 241−245.

(24) Axelsson, P. Current role of pharmaceuticals in prevention of caries and periodontal disease. *Int. Dent. J.* **1993**, *43*, 473.

(25) Sayilkan, F.; Asilturk, M.; Kiraz, N.; Tatar, N.; Arpac, E.; Sayilkan, H. Photocatalytic performance of Sn-doped TiO_2 nanostructured mono and double layer thin films for malachite green dye degradation under UV and vis-lights. *J. Hazard. Mater.* **2007**, *144*, 140.

(26) Sayilkan, F.; Asilturk, M.; Kiraz, N.; Burunkaya, E.; Arpac, E.; Sayilkan, H. Photocatalytic antibacterial performance of Sn 4+−doped TiO2 thin films on glass substrate. *J. Hazard. Mater.* **2009**, *162*, 1309−1316.

(27) Dubovoy, V.; Ganti, A.; Zhang, T.; Al-Tameemi, H.; Cerezo, J. D.; Boyd, J. M.; Asefa, T. One-pot hydrothermal synthesis of benzalkonium-templated mesostructured silica antibacterial agents. *J. Am. Chem. Soc.* **2018**, *140*, 13534−13537.

(28) Mann, R.; Dickin, F. J.; Wang, M.; Dyakowski, T.; Williams, R. A.; Edwards, R. B.; Forrest, A. E.; Holden, P. J. Application of electrical resistance tomography to interrogate mixing processes at plant scale. *Chem. Eng. Sci.* **1997a**, *52*, 2087−2097.

(29) Kaminoyama, M.; Kato, K.; Misumi, R.; Nishi, K. Measurements of the phase inversion phenomenon in a suspension polymerization reactor with an electrical resistance tomography system. *J. Chem. Eng. Japan* **2010**, *43*, 52−55.

(30) Rodgers, T. L.; Stephenson, D. R.; Cooke, M.; York, T. A.; Mann, R. Tomographic imaging during semi-batch reactive precipitation of barium sulphate in a stirred vessel. *Chem. Eng. Res. Des.* **2009**, *87*, 615−626.

(31) Stanley, S. J. Tomographic imaging during reactive precipitation in a stirred vessel: Mixing with chemical reaction. *Chem. Eng. Sci.* **2006**, *61*, 7850−7863.

(32) Bolton, G. T.; Bennett, M.; Wang, M.; Qiu, C.; Wright, M.; Primrose, K.; Stanley, S. J.; Rhodes, D. Development of an electrical tomographic system for operation in a remote, acidic and radioactive environment. *Chem. Eng. J.* **2007**, *130*, 165−169.

(33) Bolton, G. T.; Hooper, C. W.; Mann, R.; Stitt, E. H. Flow distribution and velocity measurement in a radial flow fixed bed reactor using electrical resistance tomography. *Chem. Eng. Sci.* **2004**, *59*, 1989−1997.

(34) Sharifi, M.; Young, B. Qualitative visualization and quantitative analysis of milk flow using electrical resistance tomography. *J. Food Eng.* **2012c**, *112*, 227−242.

(35) Pakzad, L.; Ein-Mozaffari, F.; Chan, P. Measuring mixing time in the agitation of non-Newtonian fluids through electrical resistance tomography. *Chem. Eng. Technol.* **2008a**, *31*, 1838−1845.

(36) Pakzad, L.; Ein-Mozaffari, F.; Upreti, S. R.; Lohi, A. Characterization of the mixing of non-newtonian fluids with a scaba 6SRGT impeller through ERT and CFD. *Can. J. Chem. Eng.* **2012**, *91*, 90−100.

(37) Bawadi, A.; Dave, C.; Nguyen, T.; Cooper, C.; Adesina, A. A. Electrical resistance tomography-assisted analysis of dispersed phase

(38) hold-up in a gas-inducing mechanically stirred vessel. *Chem. Eng. Sci.* **2011**, *66*, 5648−5662.

(38) Rodgers, T. L.; Gangolf, L.; Vannier, C.; Parriaud, M.; Cooke, M. Mixing times for process vessels with aspect ratios greater than one. *Chem. Eng. Sci.* **2011a**, *66*, 2935−2944.

(39) Paglianti, A.; Maluta, F.; Montante, G. Particles dissolution and liquid mixing dynamics by electrical resistance tomography. *Trans. Inst. Meas. Control* **2019**, *42*, 647−654.

(40) Carletti, C.; Bikić, S.; Montante, G.; Paglianti, A. Mass transfer in dilute solid-liquid stirred tanks. *Ind. Eng. Chem. Res.* **2018**, *57*, 6505−6515.

(41) Bruker. *SAINT-V8.35A. Data Reduction Software*, 2016.

(42) Sheldrick, G. M. *SADABS. Program for Empirical Absorption Correction.* University of Gottingen, Germany, 2016.

(43) Bruker. *APEX3* (Version 2015.9). Bruker AXS Inc., Madison, Wisconsin, USA, 2016.

(44) Sheldrick, G. M. Crystal structure refinement with SHELXL. *Acta Crystallogr., Sect. C: Struct. Chem.* **2015**, *C71*, 3−8.

(45) Sheldrick, G. M. Phase annealing in SHELX-90: direct methods for larger structures. *Acta Crystallogr., Sect. A: Found. Crystallogr.* **1990**, *A46*, 467−473.

(46) Sheldrick, G. M. A short history of SHELX. *Acta Crystallogr., Sect. A: Found. Crystallogr.* **2008**, *A64*, 112−122.

(47) Dolomanov, O. V.; Bourhis, L. J.; Gildea, R. J.; Howard, J. A. K.; Puschmann, H. OLEX2: A complete structure solution, refinement and analysis program. *J. Appl. Crystallogr.* **2009**, *42*, 339−341.

(48) Teoman, B.; Sirasitthichoke, C.; Potanin, A.; Armenante, P. M. Determination of the just-suspended speed, Njs, in stirred tanks using electrical resistance tomography (ERT). *AIChE J.* **2021**, *67*, No. e17354.

(49) Mosharraf, M.; Nyström, C. The effect of particle size and shape on the surface specific dissolution rate of microsized practically insoluble drugs. *Int. J. Pharm.* **1995**, *122*, 35−47.

(50) Higuchi, W. I.; Rowe, E. L.; Hiestand, E. N. Dissolution rates of finely divided drug powders II. Micronized methylprednisolone. *J. Pharm. Sci.* **1963**, *52*, 162−164.

(51) Wang, J.; Flanagan, D. R. General solution for diffusion-controlled dissolution of spherical particles. 1. Theory. *J. Pharm. Sci.* **1999**, *88*, 731−738.

(52) Wang, J.; Flanagan, D. R. General solution for diffusion-controlled dissolution of spherical particles. 2. Evaluation of experimental data. *J. Pharm. Sci.* **2002**, *91*, 534−542.

(53) Müller, U.; Mronga, N.; Schumacher, C.; Dehnicke, K. Die Kristallstrukturen von PPh4[SnCl3] und PPh4[SnBr3]/ The Crystal Structures of PPh4[SnCl3] and PPh4[SnBr3]. *Z. Naturforsch. B* **1982**, *37*, 1122−1126.

(54) Nelson, J. H.; Wilson, W. L.; Cary, L. W.; Alcock, N. W.; Clase, H. J.; Jas, G. S.; Ramsey-Tassin, L.; Kenney, J. W. Comparison of the properties of SnCl3− and SnBr3− complexes of Platinum(II). *Inorg. Chem.* **1996**, *35*, 883−892.

(55) Chouaib, H.; Kamoun, S.; Costa, L. C.; Graça, M. P. F. Synthesis, crystal structure and electrical properties of N,N-dimethylanilinium trichloridostannate (II): (C8H12N)SnCl3. *J. Mol. Struct.* **2015**, *1102*, 71−80.

(56) Garralda, M. A.; Pinilla, E.; Monge, M. A. Crystal structure of [Rh(SnCl3) (norbornadiene) (dppp)]. A 1H NMR study of [Rh(SnCl3) (norbornadiene) (diphosphine)] complexes. *J. Organomet. Chem.* **1992**, *427*, 193−200.

(57) Leung, W.-P.; Kwok, W.-H.; Xue, F.; Mak, T. C. W. Synthesis and crystal structure of an unprecedented Tin(II)−Tin(II) donor-acceptor complex, RN2SnSnCl2 [RN= CH(SiMe3)C9H6N-8]. *J. Am. Chem. Soc.* **1997**, *119*, 1145−1146.

(58) Alcock, N. W.; Nelson, J. H. The [PtCl2(SnCl3)2]2− ion: crystal structure of two salts. *J. Chem. Soc., Dalton Trans.* **1982**, *12*, 2415−2418.

(59) Ito, T.; Mikurube, K.; Abe, Y.; Koroki, T.; Saito, M.; Iijima, J.; Naruke, H.; Ozeki, T. Hybrid inorganic-organic crystals composed of octamolybdate isomers and pyridinium surfactant. *Chem. Lett.* **2010**, *39*, 1323−1325.

(60) Wang, Y. L.; Zheng, J. J.; Ma, L.; Wang, Y. F.; Yuan, G. M.; Ni, J. Crystal structure of bis (N-cetylpyridinium) bis (2-thioxo-1,3-dithiole-4,5-dithiolato) palladium (II), $[C_{21}H_{38}N]_2[Pd(C_3S_5)_2]$. *Kristallogr. - New Cryst. Struct.* **2010**, *225*, 131−133.

(61) Ito, T.; Yamase, T. Inorganic-organic hybrid layered crystal composed of polyoxomolybdate and surfactant with π electrons. *Chem. Lett.* **2009**, *38*, 370−371.

(62) Deng, F.-G.; Hu, B.; Sun, W.; Chen, J.; Xia, C.-G. Novel pyridinium based cobalt carbonyl ionic liquids: synthesis, full characterization, crystal structure and application in catalysis. *Dalton Trans.* **2007**, *38*, 4262−4267.

(63) Neve, F.; Crispini, A.; Armentano, S.; Francescangeli, O. Synthesis, structure, and thermotropic mesomorphism of layered N-alkylpyridinium tetrahalopalladate(II) salts. *Chem. Mater.* **1998**, *10*, 1904−1913.

(64) Neve, F.; Crispini, A.; Francescangeli, O. Structural studies on layered alkylpyridinium iodopalladate networks. *Inorg. Chem.* **2000**, *39*, 1187−1194.
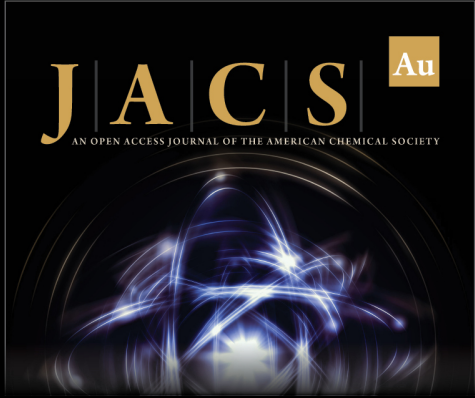
(65) Al-Tameemi, H.; Beavers, W. N.; Norambuena, J.; Skaar, E. P.; Boyd, J. M. Staphylococcus aureus lacking a functional MntABC manganese import system has increased resistance to copper. *Mol. Microbiol.* **2021**, *115*, 554−573.

(66) Boyd, J. M.; Teoh, W. P.; Downs, D. M. Decreased transport restores growth of a Salmonella enterica apbC mutant on tricarballylate. *J. Bacteriol.* **2012**, *194*, 4596−4602.

(67) Loesche, W. J. Role of streptococcus mutans in human dental decay. *Microbiol. Rev.* **1986**, *50*, 353.

■ NOTE ADDED AFTER ASAP PUBLICATION

This paper was published ASAP on December 14, 2021, with two erroneous phrases in the Abstract. The corrected version was posted on December 28, 2021.